Letter

Quantum noise as a symmetry-breaking field

Beatriz C. Dias,[1,2,3,4,*] Domagoj Perković,[1,5] Masudul Haque,[6,7,1] Pedro Ribeiro,[2,8] and Paul A. McClarty[1]

[1]*Max Planck Institute for the Physics of Complex Systems, Nöthnitzer Str. 38, 01187 Dresden, Germany*
[2]*CeFEMA, Instituto Superior Técnico, Universidade de Lisboa, Av. Rovisco Pais, 1049-001 Lisboa, Portugal*
[3]*Department of Mathematics, Technical University of Munich, 85748 Garching, Germany*
[4]*Munich Center for Quantum Science and Technology (MCQST), Munich, 80799 Munich, Germany*
[5]*Department of Physics, Cavendish Laboratory, JJ Thomson Avenue, Cambridge CB3 0HE, United Kingdom*
[6]*Institut für Theoretische Physik, Technische Universität Dresden, 01062 Dresden, Germany*
[7]*Department of Theoretical Physics, Maynooth University, Co. Kildare, Ireland*
[8]*Beijing Computational Science Research Center, Beijing 100084, China*

(Received 5 October 2022; revised 30 June 2023; accepted 30 June 2023; published 30 August 2023)

We investigate the effect of quantum noise on the measurement-induced quantum phase transition in monitored random quantum circuits. Using the efficient simulability of random Clifford circuits, we find that the transition is broadened into a crossover and that the phase diagram as a function of projective measurements and noise exhibits several distinct regimes. We show that a mapping to a classical statistical mechanics problem accounts for the main features of the random circuit phase diagram. The bulk noise maps to an explicit permutation symmetry-breaking coupling; this symmetry is spontaneously broken when the noise is switched off. These results have implications for the realization of entanglement transitions in noisy quantum circuits.

DOI: 10.1103/PhysRevB.108.L060302

Introduction. From the point of view of entanglement entropy, ground states of one-dimensional many-body quantum systems with short-range interactions mostly fall into two classes: those with area law entanglement, where entanglement entropy saturates to a constant independent of system size, and critical phases with entanglement entropy scaling as $\ln L$, with L the system's linear extent. Out of equilibrium, it also becomes possible to generate volume law entanglement and to induce area to volume law transitions. Examples have been found in disordered spin chains between thermalizing and localized phases [1–4] and in systems subject to measurements. One example of a measurement-induced entanglement transition is a spin chain under local random unitary gates and projective measurements [5–18]. In the absence of measurements, repeated application of gates to an initial product of local pure states leads to a linear build-up of the entanglement entropy [19–21] saturating at the Page value [22]. The effect of carrying out local projective measurements with rate p, in the limit where p is large, is to suppress the spread of quantum information completely so that the entanglement obeys an area law. In between there is a continuous quantum phase transition at which the volume law coefficient vanishes [5,6,8]. Measurement-induced entanglement transitions of different sorts have by now been observed in various other quantum circuits [23–33], in free fermion systems [27,34–37], in systems with continuous monitoring [34,38–43], and long-range interactions [32,36,44–48]. The weight of evidence is that these continuous phase transitions are much like their equilibrium counterparts with emergent conformal invariance and associated critical exponents, though a complete field theory description is lacking.

Since any physical system is always coupled to an environment, it is natural to ask what becomes of these measurement-induced entanglement transitions in the generic case where the system is noisy. References [27,49] made the case that quantum noise breaks down a symmetry present in the noise-free case, Refs. [43,49] studied effects of boundary noise, and Refs. [50,51] studied a model with depolarization. In this Letter, we address the effect of noise in the bulk with projective measurements applied at rate p and with some additional noise rate q. We find that the known transition at $p = p_c$, $q = 0$ is broadened and the finite p, q phase diagram exhibits three quantitatively distinct regimes separated by crossovers, Figs. 1(a) and 1(b). At small q this is reminiscent of a phase diagram where $q = 0$ displays spontaneous symmetry breaking and where q plays the role of an explicit symmetry-breaking field. We show, through a replica construction, that this picture can be made precise: the quantum noise appears as a new effective coupling in an effective classical model that explicitly breaks a replica permutation symmetry. Using the classical picture, we can account for the main features of the random circuit phase diagram. In the following, we introduce the protocol, discuss our numerical findings, and motivate a classical model that allows for their qualitative understanding.

Circuit and observables. We consider a circuit model consisting of a chain of L qudits with local Hilbert space

*Corresponding author: beatriz.dias@tecnico.ulisboa.pt

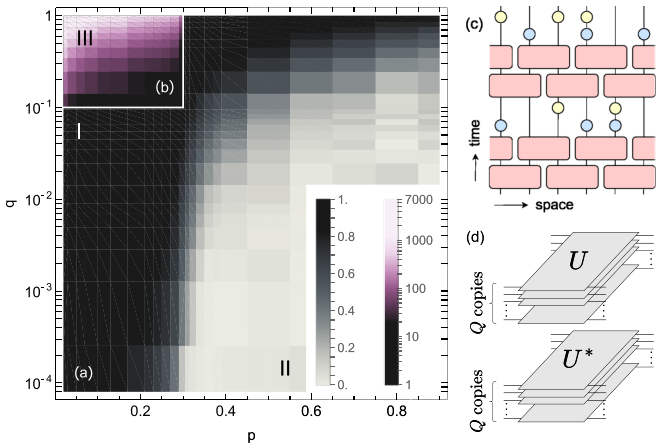

FIG. 1. (a) $|I_{AB}(L,p,q) - I_{AB}(L,p,q=0)|/I_{AB}(L,p,q=0)$ and (b) $|I_{AB}(L,p,q) - f(L,p,q)|/I_{AB}(L,p,q)$ for a system with $L = 500$. For each p, $f(L,p,q) = b(L,p)\log(1/q) + c(L,p)$ is fitted to $I_{AB}(L,p,q)$ with q in region I, where $I_{AB} \sim \log(q)$. The three marked regions correspond to $I_{AB} \sim \log(1/q)$ (I), $I_{AB} \sim q^0$ (II), and $I_{AB} \sim \exp(-q)$ (III). (c) A 1D qubit chain is evolved by applying random uniformly distributed Clifford gates (red blocks) to neighboring pairs of sites in a brick wall pattern. After each Clifford bilayer, an unmonitored measurement is performed on each site with probability q (blue circles), and then a monitored measurement is performed on each site with probability p (yellow circles). (d) The model with $p = q = 0$ has a $S_Q \times S_Q \rtimes \mathbb{Z}_2$ symmetry, where $S_Q \times S_Q$ refers to permutations of the Q copies of U and, separately, permutation of U^* while $\mathbb{Z}_2$ corresponds to swapping U and U^*. This symmetry spontaneously breaks down to $S_Q \rtimes \mathbb{Z}_2$ when $p < p_c, q = 0$ and explicitly breaks down to $S_Q \rtimes \mathbb{Z}_2$ when $q \neq 0$, $\forall p \in [0,1]$.

dimension d. Each single discrete time step of the circuit is composed of four layers [Fig. 1(c)]. The first two layers consist of local random unitary gates $\prod_r u_{2r,2r+1}$ followed by $\prod_r u_{2r-1,2r}$ in a brick wall pattern that ensures all sites communicate given enough time. After the random unitary bilayer, unmonitored measurements are performed on each site, r, with probability q. These take the state ρ to the mixed state $\sum_a M_r^{a\dagger}\rho M_r^a$, where $M_r^a = |r,a\rangle\langle r,a|$ for outcomes $a = 1,\ldots,d$ [52,53]. The final layer performs monitored (projective) measurements with probability p, taking the mixed state ρ to $M_r^{a\dagger}\rho M_r^a/\|M_r^{a\dagger}\rho M_r^a\|$ with probability $p_a = \|M_r^{a\dagger}\rho M_r^a\|$. The output state of the circuit with measurement outcomes $m = (m_1, m_2, \ldots, m_T)$ is

$$\rho_m = \sum_{\mu_1,\ldots,\mu_T=1}^{d} K_{\mu_T} M_{m_T} U_T \ldots K_{\mu_1} M_{m_1} U_1 \rho_0 \times U_1^\dagger M_{m_1}^\dagger K_{\mu_1}^\dagger \ldots U_T^\dagger M_{m_T}^\dagger K_{\mu_T}^\dagger, \quad (1)$$

where T is the circuit depth, $M_0 = \sqrt{1-p}$, $M_{i=1,\ldots,d} = p|i\rangle\langle i|$, $K_0 = \sqrt{1-q}$, and $K_{i=1,\ldots,d} = q|i\rangle\langle i|$.

We characterize the system using the entropy of subsystem A, $S_A = -\mathrm{Tr}_A(\rho_A \log \rho_A)$, with $\rho_A = \mathrm{Tr}_B\rho$ the reduced density matrix of subsystem A, obtained by tracing out its complement, B. Since the overall state of A ∪ B is no longer pure, we also consider the mutual information, $I_{AB} = S_A + S_B - S_{AB}$, with S_{AB} the entanglement entropy of the subsystem A ∪ B. We note that $I_{AB} = 2S_A$ when $q = 0$ as S_{AB} vanishes in this case.

Numerical phase diagram. In order to achieve system sizes up to a few hundred sites, we set $d = 2$ and make use of the efficient simulability of Clifford circuits with both above-mentioned single-site measurements, i.e., of stabilizer circuits [54]. As uniformly sampled gates within the stabilizer group constitute a t design of order $t = 3$ [55,56], the second Renyi entropy of local random Clifford gates with monitored and unmonitored measurements reproduce the same result as their local Haar-distributed counterpart [9,11,57]. For convenience we take an entanglement cut dividing the chain exactly in two.

We now analyze the numerical results of Figs. 1(a) and 1(b), starting from the previously known $p = 0$ line. For $p = q = 0$, the circuit as probed by local observables rapidly reaches a steady state and the entanglement entropy grows linearly saturating at a value that is proportional to L. For $q = 0$, $p = 1$, there is a projective measurement at each site for every time step so the state is a product state with short-range entanglement. There is a transition in the entanglement at $0.30 < p_c < 0.31$, $q = 0$ [58]. The entanglement entropy obeys an area law for $p > p_c$ and varies as $S_A(L, p_c, q = 0) = \beta(p_c)\log L$ at criticality. Empirically, for $p < p_c$, there is a volume law with a logarithmic correction, $S_A(L,p,q=0) = \alpha(p)L + \beta(p)\log L + \gamma(p)$, with $\lim_{p\to p_c^-}\beta(p) \neq 0$ and $\lim_{p\to p_c^+}\beta(p) = 0$, and $\alpha(p) = (p_c - p)^\nu\Theta(p_c - p)$ with $\nu \approx 1.3$ [9].

Now we turn to the finite q behavior. For $p = 0$, $q \neq 0$, the state asymptotes to the infinite temperature mixed state essentially because the unmonitored measurements proliferate branches of measurement outcomes in the density matrix leading to rapid decoherence. The circuit does not distinguish between measurement outcomes so the diagonal entries in the measurement basis become equal.

For finite p and q, the steady state density matrix is nontrivial as there is competition between branch proliferation generated by q and branch reduction driven by p. We find three distinct finite p, q regimes as indicated in the phase diagram of Fig. 1. The $q = 0$ transition is broadened into a crossover at finite q. In addition, the mutual information obeys an area law for all finite q. For $p > p_c$ and small q, the mutual information I_{AB} is q independent and equal to the area law entanglement S_{AB} for $q = 0$. In the region I of Fig. 1 (spanning $p < p_c$) and small q all the way to $p > p_c$ and large q there is a logarithmic regime $I_{AB}(L,p,q) = b(L,p)\ln(1/q) + c(L,p)$. This scaling is shown in Fig. 2(a) for $p < p_c$ and above the saturation regime for $p > p_c$ in panel (d). At the transition point itself, the finite size cuts off the logarithmic scaling at $b(L,p_c)\ln L$. We find that the coefficients $b(L,p_c)$ and $\beta(p_c)$ are compatible, as shown in Fig. 2(c). This has the important implication that the underlying correlation length grows as a power law $\xi \sim 1/q^\nu$ with exponent $\nu = 1$. For $p < p_c$, the logarithmic divergence is cut off by the volume law entanglement implying logarithmic growth of the correlation length. A third scaling regime is observed for small p and q close to 1 where I_{AB} falls off exponentially in q [59].

Mapping to a classical statistical mechanics model. The smearing of the phase transition into a crossover at finite q is reminiscent of a classical equilibrium statistical mechanics model where q explicitly breaks the symmetry that is

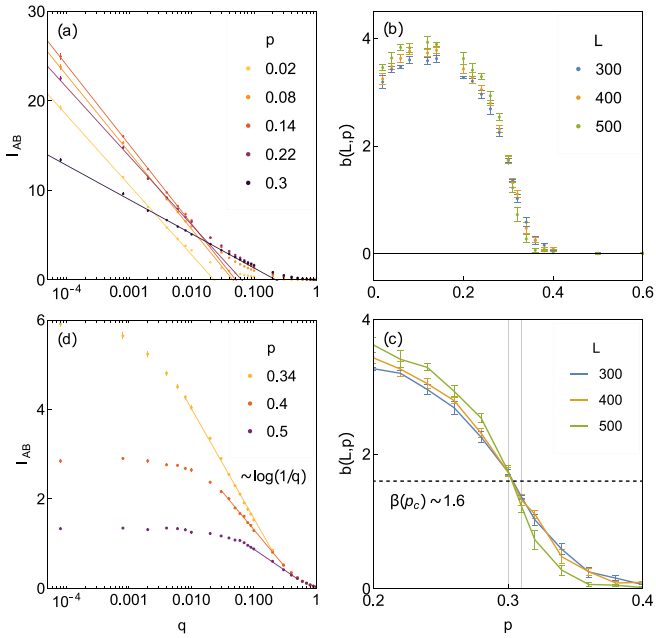

FIG. 2. (a) Mutual information, $I_{\mathrm{AB}}(q)$, for a system with $L = 500$ and for $p \in \{0.02, 0.08, 0.14, 0.22, 0.3\}$. Solid lines are $f(L, p) = b(L, p)\log(1/q) + c(L, p)$ fits to the points with $q = 0.00008, 0.0008, 0.002, 0.004$. (b) Parameter $b(L, p)$ of the fit in (a). (c) Zoom in of (b): the critical point of the transition at $q = 0$ is $p_c \in [0.30, 0.31]$. The horizontal dashed line is $\beta(p_c) \sim 1.6$ [9] in $S_{\mathrm{A}}(L, p, q = 0) = \alpha(p)L + \beta(p)\log L + \gamma(p)$. (d) Mutual information, $I_{\mathrm{AB}}(q)$, for a system with $L = 500$ and for $p \in \{0.34, 0.4, 0.5\}$. Solid lines are $b(L, p)\log(1/q) + c(L, p)$ fits to the points in region I of Fig. 1. One can see that $I_{\mathrm{AB}}(q) \sim q^0$ for small q.

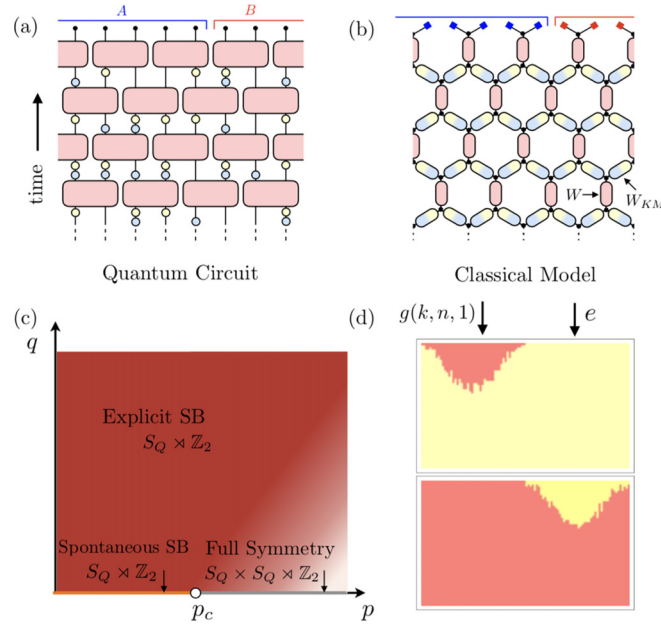

FIG. 3. Top: mapping from the quantum random circuit (a) with both projective and unmonitored measurements to a classical model with permutation degrees of freedom living on the sites of an anisotropic honeycomb lattice (b). The vertical bonds carry weights coming from the random unitaries and the half-shaded bonds carry weights depending on p and q. Panel (c) is the schematic phase diagram arising from the classical model. Panel (d) shows two domain wall configurations with pinning on the upper boundary to $g(k, n, 1)$ on the left and e on the right. In the spontaneously broken phase both configurations can arise with equal weight whereas in the explicitly broken phase the state is biased towards the upper plot with e across the system.

spontaneously broken by tuning p. We now make this connection more concrete by mapping the p, q model to a classical statistical mechanics problem building on work from Ref. [60] for random unitary circuits and Ref. [14] for the $q = 0$ model. It will turn out that this mapping accounts for many other features of the p, q phase diagram.

For this section, we generalize the qubit (two states per site) model considered above to a model of qudits (d states per site). We consider the nth Rényi entropy $S_A^{(n)} = 1/(1-n)\ln[\mathrm{Tr}_A(\rho_A^n)]$, averaged over Haar random unitaries $\{U\}$ within each layer of the circuit and measurement outcomes, $\mathbf{m}$, taken to include both monitored and unmonitored measurements

$$\bar{S}_A^{(n)} = \int dU \sum_{\mathbf{m}} \frac{1}{1-n} \ln\left[\frac{\mathrm{Tr}_A\left(\rho_{A,\mathbf{m}}^n\right)}{\mathrm{Tr}(\rho_{\mathbf{m}})^n}\right] \mathrm{Tr}(\rho_{\mathbf{m}}). \quad (2)$$

We introduce the swap operator $\Sigma_A^{(n)} = \sum_{[i]} |i^A_{g^n_{\mathrm{cyc}}(1)} i^B_1, \ldots, i^A_{g^n_{\mathrm{cyc}}(n)} i^B_n\rangle\langle i^A_1 i^B_1, \ldots, i^A_n i^B_n|$, which performs a cyclic permutation of n replicas on A while leaving B sites invariant. We also use the identity $\ln x = \lim_{k\to 0} \frac{x^k - 1}{k}$ to rewrite the logarithms, introducing an additional replica index k, giving

$$\bar{S}_A^{(n,k)} = \frac{1}{k(1-n)} \mathrm{Tr}\left\{\left[\Sigma_{n,A}^{\otimes k} \otimes 1 - 1^{\otimes(nk+1)}\right]\left[\int dU \sum_m \rho_m^{\otimes(nk+1)}\right]\right\}. \quad (3)$$

In this form one may integrate over the random unitaries and the measurement outcomes. Details are spelled out in [59]. Here we report the outcome of the averaging.

It turns out that $\bar{S}_A^{(n,k)}$ is related to the free energy cost of a domain wall in a classical statistical mechanics model [60]. This classical lattice model has degrees of freedom g_i on each site, which are elements of the permutation group $\mathcal{S}_Q$ of $Q \equiv kn + 1$ objects. The partition sum is

$$\mathcal{Z}_A = \sum_{\{g_i \in S_Q\}} \left[\prod_{\langle i,j\rangle \in \mathcal{E}_{\mathrm{V}}} W\left(g_i g_j^{-1}\right) \prod_{\langle i,j\rangle \in \mathcal{E}_{ZZ}} W_{KM}(g_i, g_j) \times \prod_{i\in\partial_0} d^{|g_i|} \prod_{i\in\partial_T\cap B} d^{|g_i|} \prod_{i\in\partial_T\cap A} d^{|g(n,k,1)^{-1} g_i|}\right]. \quad (4)$$

The anisotropic couplings are between nearest neighbors on a honeycomb lattice [Fig. 3(b)]. With i, j as neighboring honeycomb sites and $\mathcal{E}_{\mathrm{V}}$ denoting the vertical bonds and $\mathcal{E}_{ZZ}$ the zigzag bonds, the $W(g_i^{-1} g_j)$ act on the $\mathcal{E}_{\mathrm{V}}$ bonds. These are Weingarten functions originating from the average over unitaries. On the $\mathcal{E}_{ZZ}$ bonds, the weights for $q = 0$ are $W_{KM}(g, g')|_{q=0} = (1-p)^Q d^{|g^{-1}g'|} + p^Q d^Q$. Here $|g|$ means the number of cycles in permutation g. The second line in Eq. (4) consists of the boundary conditions that bias permutation degrees of freedom towards the trivial permutation on the early

and late time boundaries except along A where they are fixed to permutation $g(n,k,1)$ [59]. Crucially, boundaries aside, the model has a global $S_Q \times S_Q \rtimes \mathbb{Z}_2$ symmetry illustrated in Fig. 1(d). The U and U^* originate from the two copies that appear $Q = nk+1$ times when computing the nth Rényi entropy with k replicas. The physics is invariant under permutations of both sets of Q replicas and under the swap symmetry between the U and U^*. From Eq. (4) and weights one sees that, for large p, the local degrees of freedom fluctuate wildly while, for small p, permutations on neighboring bonds tend to lock together breaking one of the global permutation symmetries. In fact, there is a critical p, analogous to temperature, below which there is long-range order that spontaneously breaks the symmetry down to $S_Q \rtimes \mathbb{Z}_2$.

In the mapping we note that the quantum model is recovered in the $Q \to 1$ replica limit. In this context, we briefly mention one further case of interest where the probability of an outcome is taken to be independent of the state and a postselection is carried out over all circuits for a fixed set of measurement outcomes. This "forced measurement" scenario also has a measurement-induced transition. The major difference in the classical mapping when the measurements are forced is a simplification: the Born probability is not considered so the parameter $Q = rn$ instead of $rn+1$ meaning that the physical replica limit is $Q \to 0$ [26].

One may now understand features of the two phases from the classical model as the averaged replicated Rényi entropy is $\bar{S}_A^{(n,k)} = \frac{n}{1-n}\frac{\mathcal{Z}_A - \mathcal{Z}_\emptyset}{Q-1}$ where $\mathcal{Z}_A$ is defined in Eq. (4) and $\mathcal{Z}_\emptyset$ has homogeneous boundary conditions corresponding to $A \to \emptyset$. The averaged Rényi entropy is related to the free energy cost, $F_A - F_\emptyset$, of a domain wall in the statistical mechanics model via $\bar{S}_A^{(n)} = \lim_{Q\to 1} \bar{S}_A^{(n,k)} = \lim_{k\to 0} \frac{F_A - F_\emptyset}{k(n-1)}$, with $F_A = \log(\mathcal{Z}_A)$ and $F_\emptyset = \log(\mathcal{Z}_\emptyset)$. In fact, the averaged Rényi entropy is the free energy cost of a domain wall with fixed permutations [Fig. 3(d) unbiased between the two configurations shown]. Evidently, this costs $O(L)$ in the ordered phase and $O(L^0)$ in the paramagnetic phase corresponding to the volume and area law phases, respectively.

One may extend this calculation to include the unmonitored measurements. The weights W_{KM} then become

$$W_{KM}(g_i, g_j) = (1-p)^Q \Bigg[(1-q)^Q d^{|gg'^{-1}|} + \sum_{l=1}^{Q} q^l (1-q)^{Q-l} \times \sum_{\{r_1,\ldots,r_l\}\in B_{l,Q}} d^{|gg'^{-1} h_{r_1}^{t_1} \ldots h_{r_l}^{t_l}|} \Bigg] + p^Q d^Q, \tag{5}$$

where $B_{l,Q}$ is the set of subsets of $1,2,\ldots,Q$ with l elements and where $h_r = [g^{-1}(r)\ r]$ is a two cycle that permutes replica index r and $g^{-1}(r)$ and $t_k = 1/2 + \mathrm{sgn}(|gg'^{-1}| - |gg'^{-1}h_{r_k}|)/2$, is either 0 or 1. Despite the notational complexity, the h_r insertions have a relatively simple effect. That is to say if, in the permutation gg'^{-1}, the elements $g^{-1}(r)$ and r belong to different cycles, then $gg'^{-1}h_{r_k}^{t_k}$ joins the cycles to which $g^{-1}(k)$ and k belong and $|gg'^{-1}| - |gg'^{-1}h_{r_k}| = 1$. If the elements $g^{-1}(k)$ and k already belong to the same cycle, then $|gg'^{-1}| - |gg'^{-1}h_{r_k}| = -1$ and $t_k = 0$, such that $gg'^{-1}h_{r_k}^{t_k} = gg'^{-1}$. Overall, Eq. (5) reduces to the $q = 0$ weight quoted above.

Comparison of classical picture and quantum model. We can now interpret the random circuit results from the point of view of the classical model. The primary effect of introducing quantum noise is an explicit breaking of the symmetry of the model down to $S_Q \rtimes \mathbb{Z}_2$ to which, we recall, it is spontaneously broken when $q = 0$. In one sense, one of the global permutation symmetries is broken as quantum noise locks together U and U^* copies. We may understand the explicit symmetry breaking from another perspective by inspecting the large d, small q limit. In this limit, the $q = 0$ model reduces to a $Q!$ state Potts model that for $Q > 2$ displays a first-order phase transition and for $Q \leqslant 2$ a continuous phase transition [61]. Expanding Eq. (5) linearly in q and collecting the largest powers of d we obtain [59]

$$W_{KM}(g_i, g_j) = d^Q((1-p)^Q[(1-q) + q|g_j|_1]\delta_{g_i,g_j} + p^Q), \tag{6}$$

where $|g|_1$ denotes the number of one cycles in g. Thus the leading effect of q is to pick out the permutation with the largest number of cycles—the trivial permutation from all $Q!$ states equivalent to applying directly a symmetry-breaking field that biases the system towards the e permutation with an extensive contribution to the free energy [Fig. 3(d), now biased towards the upper configuration].

Thus, for finite p, quantum noise drives the system to the infinite temperature fixed point of the classical model. This accounts for the most prominent feature of the phase diagram: the smearing of the transition into a crossover for $q \neq 0$. For $p = 0$, the system instead flows to the infinite-field fixed point corresponding to the maximally mixed state.

Turning to the observables, we note that S_{AB} vanishes for $q = 0$ but exhibits a volume law for $q \neq 0$. From the point of view of the classical model, when $q = 0$, S_{AB} is the free energy difference of a system with boundary degrees of freedom pinned to a nontrivial permutation across the entire system and a system with a boundary pinned to the trivial permutation [Fig. 3(d)]. But, for $q = 0$, the free energy is indifferent to the precise pinning field so the free energy difference must vanish. This ceases to be the case when $q \neq 0$ because q distinguishes the trivial permutation leading to an $O(L)$ free energy difference as observed in the quantum model. A similar argument allows us to understand why I_{AB} has an area law for $q \neq 0$: the domain wall cost is a constant α times L in S_{AB} which is canceled off by the two $\alpha L/2$ contributions in S_A and S_B.

Finally the classical model provides some insight into the $\log q$ dependence of the mutual information. In the vicinity of the $q = 1$ line, one may carry out the analog of a high temperature expansion with Boltzmann weights $\exp(c \log q)$. Since q is close to 1, the appropriate expansion parameter is $\log q$. Then for $p < p_c$, the only further scale that enters the problem is L but until this cutoff is reached there is nothing to interfere with the $\log q$ growth from the high temperature expansion.

Discussion and conclusion. We have introduced and studied a random circuit model subjected to both projective and unmonitored measurements. We have shown that, at finite q, the transition known for projective-only measurements ($q = 0$) is washed out and the phase diagram is reminiscent of that

of a finite temperature ferromagnet with q playing the role of an applied field. We have made this connection precise through a mapping to a classical statistical mechanics model with finite replica index Q (the quantum model corresponding to replica index $Q \to 1$). In the classical model, q explicitly breaks down the global permutation symmetry of the model to $S_Q \rtimes \mathbb{Z}_2$. Thus, quantum noise (originating, e.g., from coupling to a bath) is a relevant operator driving the system to the infinite temperature fixed point. We have seen that various features of the quantum model follow from the classical statistical mechanics analog. It is amusing to note that the passage from pure to mixed states by switching on q is reflected in the classical model as a field that affects the response of the system but not the state space. Indeed, in the classical model the difference between the pure and mixed states is only apparent through boundary conditions.

What is the broader significance of the main result of this Letter? All quantum systems are subject to quantum noise coming from the environment. Our result suggests that, in a realistic setting, the entanglement transition driven by monitored measurements will be smeared out by the environment. In addition, our work shows that nonequilibrium mixed state dynamics in Hilbert space in the presence of a quantum bath can be viewed as breaking a delicate symmetry that is only present for pure states. It would be of considerable interest to devise a model with an entanglement transition in the presence of bulk noise [10]. Whether this is possible or not has a bearing on the experimental simulability of these entanglement transitions as well as implications for error-corrected quantum computers [62].

Acknowledgments. B.D. and P.R. acknowledge MPI PKS where part of this work was carried out. B.D. acknowledges support by the European Research Council under Grant Agreement No. 101001976 (project EQUIPTNT).

[1] D. A. Abanin, E. Altman, I. Bloch, and M. Serbyn, *Colloquium*: Many-body localization, thermalization, and entanglement, Rev. Mod. Phys. **91**, 021001 (2019).

[2] R. Nandkishore and D. A. Huse, Many-body localization and thermalization in quantum statistical mechanics, Annu. Rev. Condens. Matter Phys. **6**, 15 (2015).

[3] S. A. Parameswaran and R. Vasseur, Many-body localization, symmetry and topology, Rep. Prog. Phys. **81**, 082501 (2018).

[4] F. Alet and N. Laflorencie, Many-body localization: An introduction and selected topics, C. R. Phys. **19**, 498 (2018).

[5] Y. Li, X. Chen, and M. P. A. Fisher, Quantum Zeno effect and the many-body entanglement transition, Phys. Rev. B **98**, 205136 (2018).

[6] A. Chan, R. M. Nandkishore, M. Pretko, and G. Smith, Unitary-projective entanglement dynamics, Phys. Rev. B **99**, 224307 (2019).

[7] R. Vasseur, A. C. Potter, Y.-Z. You, and A. W. W. Ludwig, Entanglement transitions from holographic random tensor networks, Phys. Rev. B **100**, 134203 (2019).

[8] B. Skinner, J. Ruhman, and A. Nahum, Measurement-Induced Phase Transitions in the Dynamics of Entanglement, Phys. Rev. X **9**, 031009 (2019).

[9] Y. Li, X. Chen, and M. P. A. Fisher, Measurement-driven entanglement transition in hybrid quantum circuits, Phys. Rev. B **100**, 134306 (2019).

[10] S. Choi, Y. Bao, X.-L. Qi, and E. Altman, Quantum Error Correction in Scrambling Dynamics and Measurement-Induced Phase Transition, Phys. Rev. Lett. **125**, 030505 (2020).

[11] M. J. Gullans and D. A. Huse, Dynamical Purification Phase Transition Induced by Quantum Measurements, Phys. Rev. X **10**, 041020 (2020).

[12] Y. Bao, S. Choi, and E. Altman, Theory of the phase transition in random unitary circuits with measurements, Phys. Rev. B **101**, 104301 (2020).

[13] Q. Tang and W. Zhu, Measurement-induced phase transition: A case study in the nonintegrable model by density-matrix renormalization group calculations, Phys. Rev. Res. **2**, 013022 (2020).

[14] C.-M. Jian, Y.-Z. You, R. Vasseur, and A. W. W. Ludwig, Measurement-induced criticality in random quantum circuits, Phys. Rev. B **101**, 104302 (2020).

[15] A. Zabalo, M. J. Gullans, J. H. Wilson, S. Gopalakrishnan, D. A. Huse, and J. H. Pixley, Critical properties of the measurement-induced transition in random quantum circuits, Phys. Rev. B **101**, 060301(R) (2020).

[16] R. Fan, S. Vijay, A. Vishwanath, and Y.-Z. You, Self-organized error correction in random unitary circuits with measurement, Phys. Rev. B **103**, 174309 (2021).

[17] P. Sierant and X. Turkeshi, Universal Behavior beyond Multifractality of Wave Functions at Measurement-Induced Phase Transitions, Phys. Rev. Lett. **128**, 130605 (2022).

[18] A. Zabalo, M. J. Gullans, J. H. Wilson, R. Vasseur, A. W. W. Ludwig, S. Gopalakrishnan, D. A. Huse, and J. H. Pixley, Operator Scaling Dimensions and Multifractality at Measurement-Induced Transitions, Phys. Rev. Lett. **128**, 050602 (2022).

[19] A. Nahum, J. Ruhman, S. Vijay, and J. Haah, Quantum Entanglement Growth under Random Unitary Dynamics, Phys. Rev. X **7**, 031016 (2017).

[20] C. W. von Keyserlingk, T. Rakovszky, F. Pollmann, and S. L. Sondhi, Operator Hydrodynamics, OTOCs, and Entanglement Growth in Systems without Conservation Laws, Phys. Rev. X **8**, 021013 (2018).

[21] A. Nahum, S. Vijay, and J. Haah, Operator Spreading in Random Unitary Circuits, Phys. Rev. X **8**, 021014 (2018).

[22] D. N. Page, Average Entropy of a Subsystem, Phys. Rev. Lett. **71**, 1291 (1993).

[23] J. Iaconis, A. Lucas, and X. Chen, Measurement-induced phase transitions in quantum automaton circuits, Phys. Rev. B **102**, 224311 (2020).

[24] X. Turkeshi, R. Fazio, and M. Dalmonte, Measurement-induced criticality in $(2+1)$-dimensional hybrid quantum circuits, Phys. Rev. B **102**, 014315 (2020).

[25] A. Lavasani, Y. Alavirad, and M. Barkeshli, Measurement-induced topological entanglement transitions in symmetric random quantum circuits, Nat. Phys. **17**, 342 (2021).

[26] A. Nahum, S. Roy, B. Skinner, and J. Ruhman, Measurement and Entanglement Phase Transitions in All-To-All Quantum Circuits, on Quantum Trees, and in Landau-Ginsburg Theory, PRX Quantum **2**, 010352 (2021).
[27] Y. Bao, S. Choi, and E. Altman, Symmetry enriched phases of quantum circuits, Ann. Phys. **435**, 168618 (2021).
[28] M. Ippoliti, M. J. Gullans, S. Gopalakrishnan, D. A. Huse, and V. Khemani, Entanglement Phase Transitions in Measurement-Only Dynamics, Phys. Rev. X **11**, 011030 (2021).
[29] M. Szyniszewski, A. Romito, and H. Schomerus, Entanglement transition from variable-strength weak measurements, Phys. Rev. B **100**, 064204 (2019).
[30] S. Sang and T. H. Hsieh, Measurement-protected quantum phases, Phys. Rev. Res. **3**, 023200 (2021).
[31] A. Lavasani, Y. Alavirad, and M. Barkeshli, Topological Order and Criticality in $(2+1)$D Monitored Random Quantum Circuits, Phys. Rev. Lett. **127**, 235701 (2021).
[32] M. Block, Y. Bao, S. Choi, E. Altman, and N. Y. Yao, Measurement-Induced Transition in Long-Range Interacting Quantum Circuits, Phys. Rev. Lett. **128**, 010604 (2022).
[33] Y. Han and X. Chen, Measurement-induced criticality in $\mathbb{Z}_2$-symmetric quantum automaton circuits, Phys. Rev. B **105**, 064306 (2022).
[34] O. Alberton, M. Buchhold, and S. Diehl, Entanglement Transition in a Monitored Free-Fermion Chain: From Extended Criticality to Area Law, Phys. Rev. Lett. **126**, 170602 (2021).
[35] M. Buchhold, Y. Minoguchi, A. Altland, and S. Diehl, Effective Theory for the Measurement-Induced Phase Transition of Dirac Fermions, Phys. Rev. X **11**, 041004 (2021).
[36] S.-K. Jian, C. Liu, X. Chen, B. Swingle, and P. Zhang, Measurement-Induced Phase Transition in the Monitored Sachdev-Ye-Kitaev Model, Phys. Rev. Lett. **127**, 140601 (2021).
[37] B. Ladewig, S. Diehl, and M. Buchhold, Monitored open fermion dynamics: Exploring the interplay of measurement, decoherence, and free Hamiltonian evolution, Phys. Rev. Res. **4**, 033001 (2022).
[38] X. Cao, A. Tilloy, and A. D. Luca, Entanglement in a fermion chain under continuous monitoring, SciPost Phys. **7**, 024 (2019).
[39] M. Szyniszewski, A. Romito, and H. Schomerus, Universality of Entanglement Transitions from Stroboscopic to Continuous Measurements, Phys. Rev. Lett. **125**, 210602 (2020).
[40] Y. Fuji and Y. Ashida, Measurement-induced quantum criticality under continuous monitoring, Phys. Rev. B **102**, 054302 (2020).
[41] X. Turkeshi, M. Dalmonte, R. Fazio, and M. Schirò, Entanglement transitions from stochastic resetting of non-Hermitian quasiparticles, Phys. Rev. B **105**, L241114 (2022).
[42] Y. Minoguchi, P. Rabl, and M. Buchhold, Continuous Gaussian measurements of the free boson CFT: A model for exactly solvable and detectable measurement-induced dynamics, SciPost Phys. **12**, 009 (2022).
[43] X. Turkeshi, L. Piroli, and M. Schiró, Enhanced entanglement negativity in boundary-driven monitored fermionic chains, Phys. Rev. B **106**, 024304 (2022).
[44] T. Minato, K. Sugimoto, T. Kuwahara, and K. Saito, Fate of Measurement-Induced Phase Transition in Long-Range Interactions, Phys. Rev. Lett. **128**, 010603 (2022).
[45] S. Sharma, X. Turkeshi, R. Fazio, and M. Dalmonte, Measurement-induced criticality in extended and long-range unitary circuits, SciPost Phys. Core **5**, 023 (2022).
[46] T. Hashizume, G. Bentsen, and A. J. Daley, Measurement-induced phase transitions in sparse nonlocal scramblers, Phys. Rev. Res. **4**, 013174 (2022).
[47] T. Müller, S. Diehl, and M. Buchhold, Measurement-Induced Dark State Phase Transitions in Long-Ranged Fermion Systems, Phys. Rev. Lett. **128**, 010605 (2022).
[48] P. Sierant, G. Chiriacò, F. M. Surace, S. Sharma, X. Turkeshi, M. Dalmonte, R. Fazio, and G. Pagano, Dissipative Floquet dynamics: From steady state to measurement induced criticality in trapped-ion chains, Quantum **6**, 638 (2022).
[49] Z. Weinstein, Y. Bao, and E. Altman, Measurement-Induced Power-Law Negativity in an Open Monitored Quantum Circuit, Phys. Rev. Lett. **129**, 080501 (2022).
[50] Z. Li, S. Sang, and T. H. Hsieh, Entanglement dynamics of noisy random circuits, Phys. Rev. B **107**, 014307 (2023).
[51] K. Noh, L. Jiang, and B. Fefferman, Efficient classical simulation of noisy random quantum circuits in one dimension, Quantum **4**, 318 (2020).
[52] M. Nielsen and I. Chuang, *Quantum Computation and Quantum Information* (Cambridge University Press, Cambridge, UK, 2010).
[53] D. A. Lidar, Lecture notes on the theory of open quantum systems, arXiv:1902.00967.
[54] S. Aaronson and D. Gottesman, Improved simulation of stabilizer circuits, Phys. Rev. A **70**, 052328 (2004).
[55] Z. Webb, The Clifford group forms a unitary 3-design, Quantum Inf. Comput. **16**, 1379 (2016).
[56] H. Zhu, Multiqubit Clifford groups are unitary 3-designs, Phys. Rev. A **96**, 062336 (2017).
[57] E. Van Den Berg, A simple method for sampling random Clifford operators, in *2021 IEEE International Conference on Quantum Computing and Engineering (QCE)* (IEEE Computer Society, Los Alamitos, CA, USA, 2021), pp. 54–59.
[58] The reported value in Ref. [5] is approximately half of this value, i.e., $p_c = 0.16$, because their circuit has one measurement layer for each (even or odd) unitary layer.
[59] See Supplemental Material at http://link.aps.org/supplemental/10.1103/PhysRevB.108.L060302 for further details and additional supporting data.
[60] T. Zhou and A. Nahum, Emergent statistical mechanics of entanglement in random unitary circuits, Phys. Rev. B **99**, 174205 (2019).
[61] F. Y. Wu, The Potts model, Rev. Mod. Phys. **54**, 235 (1982).
[62] D. Aharonov, Quantum to classical phase transition in noisy quantum computers, Phys. Rev. A **62**, 062311 (2000).